CHEMISTRY
AN ASIAN JOURNAL
ACES
FULL PAPER

DOI: 10.1002/asia.201300627

VIP

A Joint Photoelectron Spectroscopy and Theoretical Study on the Electronic Structure of UCl_5^- and UCl_5

Jing Su,[a] Phuong Diem Dau,[b] Chao-Fei Xu,[a] Dao-Ling Huang,[b] Hong-Tao Liu,[b] Fan Wei,[c] Lai-Sheng Wang,*[b] and Jun Li*[a, d]

Abstract: We report a combined photoelectron spectroscopic and relativistic quantum chemistry study on gaseous UCl_5^- and UCl_5. The UCl_5^- anion is produced using electrospray ionization and found to be highly electronically stable with an adiabatic electron binding energy of 4.76 ± 0.03 eV, which also represents the electron affinity of the neutral UCl_5 molecule. Theoretical investigations reveal that the ground state of UCl_5^- has an open shell with two unpaired electrons occupying two primarily U $5f_{z^3}$ and $5f_{xyz}$ based molecular orbitals. The structures of both UCl_5^- and UCl_5 are theoretically optimized and confirmed to have C_{4v} symmetry. The computational results are in good agreement with the photoelectron spectra, providing insights into the electronic structures and valence molecular orbitals of UCl_5^- and UCl_5. We also performed systematic theoretical studies on all the uranium pentahalide complexes UX_5^- (X = F, Cl, Br, I). Chemical bonding analyses indicate that the U–X interactions in UX_5^- are dominated by ionic bonding, with increasing covalent contributions for the heavier halogen complexes.

Keywords: ab initio calculations · actinides · density functional calculations · photoelectron spectroscopy · uranium

Introduction

Molten salts display some unique properties that make them important in the nuclear energy industry both as coolants and in hydrometallurgical liquid–liquid extraction for reprocessing of spent fuels.[1] Chloride-based salts, such as NaCl–KCl and LiCl–KCl melts, are used in pyrochemical nuclear applications due to their radiolytic stability and their capacity of facilitating the dissolution of oxide mixtures.[2,3] Knowledge of the electronic structures and chemical and thermodynamic properties of uranium chloride species is important to understanding the actinide chemical speciation and redox processes in molten salts.[4–7] The UCl_5^- complex was thought to be formed under excess Cl^- in molten salts,[8] but there have been few studies about its physical and chemical properties. In particular, spectroscopic studies of the isolated uranium pentachloride complexes have been hindered by its complicated chemistry at elevated temperatures.[9–11] Gruen and McBeth studied the vapor species of UCl_5 and found that it exists as a dimeric form (U_2Cl_{10}) between 450 and 650 K.[12] Lau and Hildenbrand reported the enthalpy of formation of the UCl_5 complex, yielding a bond dissociation energy $D°(Cl_4U–Cl)$ as 50 ± 2 kcal mol^{-1} at 298 K.[13] To our knowledge, the isolated UCl_5^- complex has not been observed or investigated previously.

In solid UCl_5, each uranium atom is coordinated octahedrally to six chlorine atoms.[14] Two of the chlorine ligands are bridged between U atoms to form a dimeric U_2Cl_{10} unit. The U–Cl bond lengths involving the bridging Cl are 2.67 and 2.70 Å, respectively, while those involving non-bridging Cl are about 2.44 Å. The overall geometry of UCl_5 in the dimeric U_2Cl_{10} unit is more complicated than the C_{4v} UCl_5 in the gas phase.[14,15] Core and valence X-ray photoelectron spectroscopy of uranium halide confirmed the participation of the U 5f orbitals in bonding and the enhancement of covalency for heavy halide ligands.[16] All studies of UCl_5 in the condensed phase have shown that the U atom preferred to be coordinated with more than five ligands. Hence, the synthesis of monomeric UCl_5 often involves solvent molecules as additional neutral ligands (nL), which were found

[a] Dr. J. Su, C.-F. Xu, Prof. Dr. J. Li
Department of Chemistry & Key Laboratory of Organic Optoelectronics and Molecular Engineering of Ministry of Education
Tsinghua University
Beijing 100084 (China)
E-mail: junli@mail.tsinghua.edu.cn

[b] P. D. Dau, D.-L. Huang, Dr. H.-T. Liu, Prof. Dr. L.-S. Wang
Department of Chemistry
Brown University
Providence, RI 02912 (USA)
E-mail: lai-sheng_wang@brown.edu

[c] Dr. F. Wei
Supercomputing Center of the Computer Network Information Center
Chinese Academy of Sciences
Beijing, 100190 (China)

[d] Prof. Dr. J. Li
William R. Wiley Environmental Molecular Sciences Laboratory
Pacific Northwest National Laboratory
Richland, WA 99352 (USA)

to strongly influence the electronic properties of the UCl_5·nL species.[17–20]

Spectroscopic information of isolated UCl_5 and UCl_5^- complexes in the gas phase would be valuable to validate the relativistic quantum chemistry methods developed to account for the f electrons in chemical bonding.[21–25] In particular, U is in its +5 oxidation state in UCl_5 with a ground electronic configuration of $[Rn]5f^1$, making it an ideal system to compare with theoretical calculations. Previous theoretical calculations by Hay and co-workers showed that UCl_5 has C_{4v} symmetry, similar to UF_5.[26,27] However, there have been no experimental spectroscopic data on gaseous uranium pentachloride.

We have developed a technique to study solution species in the gas phase using electrospray ionization (ESI) and photoelectron spectroscopy (PES).[28] Recently, we have successfully produced a series of uranyl (UO_2^{2+}) halide complexes using ESI and investigated their electronic structures using PES and relativistic quantum chemical calculations.[28–30] We have also been able to produce UF_5^- using ESI and obtained its PES spectra.[32] A broad vibrational progression was observed in the U-F totally symmetric mode due to the detachment of the $8a_1$ orbital ($5f_{z^3}$). Photodetachment cross-section from the primarily $5f_{xyz}$ ($2b_2$) orbital was shown to be very weak. The electron affinity (EA) of UF_5 was measured accurately as 3.885 ± 0.015 eV. In the current work, we report the first experimental observation and characterization of gaseous UCl_5^- using ESI and PES. Electron detachment features from both the 5f orbitals and the ligand orbitals are observed. The EA of UCl_5 is measured to be 4.76 ± 0.03 eV. Relativistic quantum chemical calculations are carried out and both UCl_5^- and UCl_5 are found to have C_{4v} symmetry. The electronic structure and chemical bonding are investigated and compared for all the pentahalide complexes UX_5^- (X = F, Cl, Br, I).

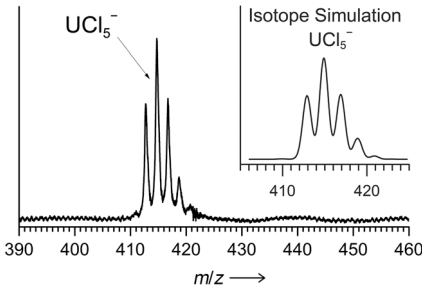

Figure 1. Mass spectrum of UCl_5^-. The inset shows the simulated isotope distribution.

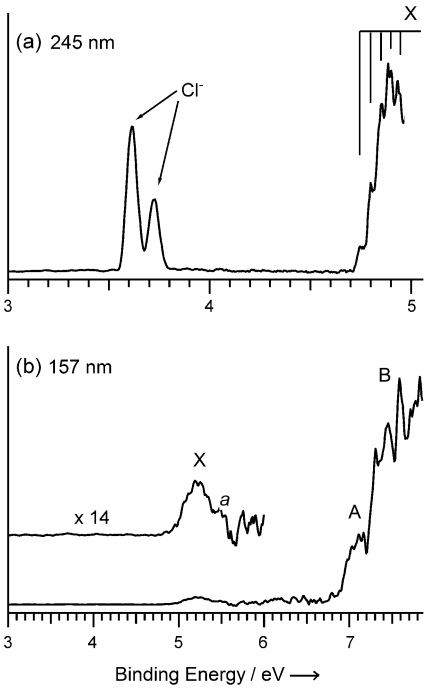

Figure 2. Photoelectron spectra of UCl_5^- at (a) 245 nm and (b) 157 nm.

Results and Discussion

Photoelectron Spectroscopy of UCl_5^-

The UCl_5^- anion was produced by electrospray ionization of a 1 mM solution of UCl_4 in acetonitrile. The anions from the ESI source were accumulated in a cryogenically-cooled ion trap operated at 20 K and then pulsed into the extraction zone of a time-of-flight mass spectrometer. The mass spectrum of UCl_5^- is shown in Figure 1 and its identification is confirmed by the simulated spectrum, as given in the inset. The PES spectra of UCl_5^- at 245 nm and 157 nm are shown in Figure 2. At 157 nm (Figure 2b), very weak signals are observed around 5 eV followed by a large energy gap (~1.9 eV) and more congested detachment bands above 7 eV. The low energy part, which should be due to detachment from the 5f electrons, is observed to contain two components, labeled as X and *a*. The X band represents the detachment transition from the ground state of UCl_5^- to that of UCl_5. The peak maximum yields a vertical detachment energy (VDE) of 5.22 eV. The weak shoulder labeled as *a* at about 5.5 eV should correspond to an excited state of UCl_5. The high binding energy features above 7 eV should correspond to detachment of primarily Cl 3p orbitals, which have much higher detachment cross-sections than the U 5f orbitals at this photon energy. The band A has a VDE of about 7.1 eV and the spectral features above 7.2 eV (labeled as B) are almost continuous, suggesting a high density of ligand orbitals.

At 245 nm (Figure 2a), only part of the X band is observed with fine vibrational features. Two sharp peaks around 3.6 eV due to Cl^- are observed, suggesting that the UCl_5^- anion can dissociate at 245 nm: $UCl_5^- \rightarrow UCl_4 + Cl^-$. The vibrational progression yields an average spacing of about 350 cm^{-1}, which should be due to the totally symmetric U–Cl vibrational mode of neutral UCl_5. Because vibrational hot bands are completely eliminated using our cold ion trap operated at 20 K, the first vibrational feature defines an accurate adiabatic detachment energy (ADE) of

4.76 ± 0.03 eV, which also represents the EA of neutral UCl_5.

The Electronic Structures of UCl_5^-

Theoretical studies were carried out using both density function theory (DFT) and ab initio wavefunction theory (WFT) methods, including the coupled-cluster with single and double and perturbative triple excitations [CCSD(T)]. Both calculations show that the ground state of UCl_5^- is a triplet state ($^3B_2$) with C_{4v} symmetry. In addition, the scalar relativistic (SR) and spin-orbit (SO) coupling effects were taken into account by zero-order-regular-approximation (ZORA) with the PBE functional (see the computational details below). The SR-ZORA and SO-ZORA calculations showed that the D_{3h} isomer of UCl_5^- is about 7.7 and 2.9 kcal mol^{-1} higher than the C_{4v} structure, respectively, suggesting a significant SO coupling effect. The SO effect is slightly larger for the D_{3h} than for the C_{4v} structure because the singly occupied SO orbitals have more character of higher angular momentum orbitals (U 5fϕ and 5fδ) in the D_{3h} than in the C_{4v} structure. The first ADE and VDE of UCl_5^- at the DFT and CCSD(T) levels with SR and SO effects are compared with the experimental data in Table 1. As observed before,[29–32] DFT/PBE calculations underestimate the electronic binding energies by 1.2–1.3 eV, while the CCSD(T) calculations are in much better agreement with the experiment.

Table 1. Calculated and observed first adiabatic (ADE) and vertical (VDE) detachment energy for UCl_5^-.

	Exp.	DFT/PBE		CCSD(T)	
		SR	SO	SR	SO[a]
ADE (eV)	4.76 ± 0.03	3.58	3.58	4.54	4.73
VDE (eV)	5.22 ± 0.06	3.93	3.93	4.99	5.18

[a] These SO results of VDE are obtained by combining the CASSCF/CR-EOM-CCSD(T)/SO and CASSCF/CCSD(T)/SO calculations; the SO result of the ADE are estimated with the SO correction for the VDE value.

The optimized ground state structural parameters of UCl_5^- and UCl_5 at DFT and CCSD(T) levels are given in Table 2. Both methods yield similar structures with less than 0.01 Å difference in the calculated bond lengths and less than 2° in the bond angle. We note that additional SO coupling corrections do not affect the bond angles, but only elongate the U–Cl bond length by 0.005 Å. Since all structural parameters calculated with SO coupling are not significantly different from the SR values, they are not included in Table 2. Overall, the computational results show that the U–Cl bond lengths are shortened by about 0.09–0.11 Å upon removal of an electron from UCl_5^-. The vibrational frequencies of the totally symmetric U–Cl stretching mode, $\nu_s(U-Cl_{ax})$, calculated at DFT/PBE are 289 and 353 cm^{-1} for the ground state of UCl_5^- and UCl_5, respectively. The calculated $\nu_s(U-Cl_{ax})$ for neutral UCl_5 is in excellent agreement with the observed vibrational spacing (~350 cm^{-1}) in the 245 nm PES spectrum (Figure 2a).

Table 2. Optimal ground-state geometrical parameters of UCl_5^- and UCl_5 at the scalar relativistic level.

	Sym	GS[a]	U–Cl_{ax} [Å]	U–Cl_{eq} [Å]	∢$Cl_{ax}UCl_{eq}$ [°]	$\nu_s(U-Cl_{ax})$ [cm^{-1}]	
			DFT/PBE				Exp.
UCl_5^-	C_{4v}	$^3B_2$	2.560	2.582	102.9	289	
UCl_5	C_{4v}	$^2B_2$	2.460	2.486	97.2	353	~350
			CCSD(T)				
UCl_5^-	C_{4v}	$^3B_2$	2.560	2.592	102.6		
UCl_5	C_{4v}	$^2B_2$	2.456	2.482	99.1		

[a] The ground state of UCl_5^- has an electron configuration of $(2b_2)^1(8a_1)^1$ and that of UCl_5 has an electron occupation of $(2b_2)^1(8a_1)^0$. See Figure 4 for the MO contour diagrams.

The valence molecular orbital (MO) energy levels for UCl_5^- are shown in Figure 3 with SR and SO effects included. Details of the calculated VDEs for all the MOs at SO-DFT/PBE can be found in Table 3. The three-dimensional iso-surface contours of the MOs from DFT calculations are presented in Figure 4. The MOs from 8e to $2b_2$ are mainly composed of U 5f orbitals, while the low-lying MOs are primarily of Cl 3p-type orbitals. The two unpaired electrons in UCl_5^- occupy the 5f-base $8a_1$ and $2b_2$ MOs, which is the SOMO (singly occupied molecular orbital). For the low-lying MOs of UCl_5^-, only the 5e orbitals display strong SO

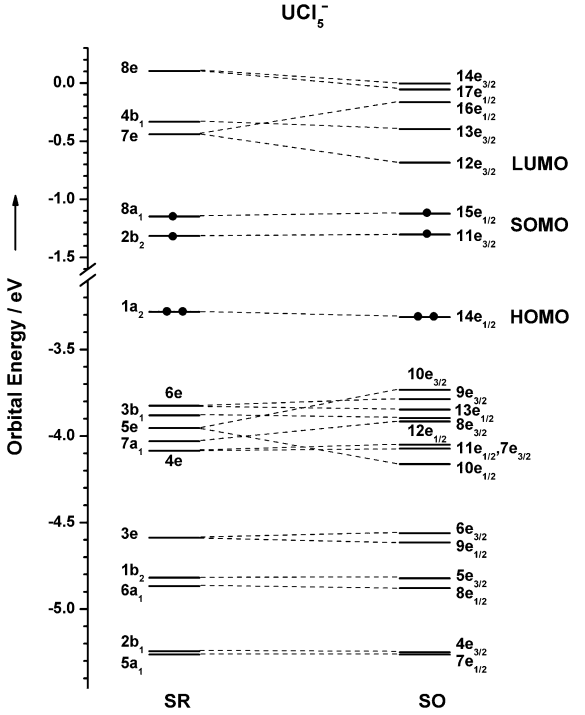

Figure 3. Qualitative SR and SO energy levels of the frontier orbitals of UCl_5^- calculated at the DFT/PBE level. The $8a_1$ and $2b_2$ orbitals are singly occupied MOs (SOMO) of mainly U 5f character, and the lower-lying orbitals are mainly Cl 3p lone pair orbitals. The virtual orbitals (8e, $4b_1$, 7e) of mainly U 5f character are also included. The SR energy levels are obtained from α spin orbitals, and the SO energy levels are from the lower spinor in each pairs of the SO split orbitals. The symmetry labels for the SO energy levels are derived from the restricted SO calculations.

Table 3. The calculated VDEs and the corresponding MOs of UCl_5^- from SO-DFT/PBE and SR CR-EOM-CCSD(T) calculations. All energies are in eV.

SO-DFT/PBE[a]			CR-EOM-CCSD(T)[b]			
VDE#	MO	VDE	VDE#	state	MO	VDE
1	$8a_1$ (U 5f)	5.18	1	X $^2B_2$	$8a_1$ (U 5f)	4.99
2	$2b_2$ (U 5f)	5.36	2	a $^2A_1$	$2b_2$ (U 5f)	5.13
3	$1a_2$ (Cl 3p)	7.35	3	a $^4B_1$	$1a_2$ (Cl 3p)	6.67
4	5e (Cl 3p)	7.81	4	a ^4E	6e (Cl 3p)	7.03
5	6e (Cl 3p)	7.89–7.90	5	a $^4A_2$	$3b_1$ (Cl 3p)	7.12
6	$3b_1$ (Cl 3p)	7.95	6	b ^4E	5e (Cl 3p)	7.23
7	$7a_1$ (Cl 3p)	7.97	7	a $^2B_1$	$1a_2$ (Cl 3p)	7.29
8	4e (Cl 3p)	8.09, 8.13	8	c ^4E	4e (Cl 3p)	7.41
9	5e (Cl 3p)	8.21	9	a $^4B_2$	$7a_1$,$6a_1$ (Cl 3p)	7.43
10	3e (Cl 3p)	8.58, 8.67	10	a ^2E	6e,5e,4e(Cl 3p)	7.76
11	$6a_1$,$1b_2$ (Cl 3p)	8.85, 8.94	11	a $^2A_2$	$3b_1$ (Cl 3p)	7.89
12	$5a_1$,$2b_1$ (Cl 3p)	9.27, 9.32	12	d ^4E	3e (Cl 3p)	8.16
			13	a $^4A_1$	$1b_2$ (Cl 3p)	8.23
			14	b $^4B_2$	$6a_1$,$5a_1$ (Cl 3p)	8.44
			15	b $^4A_2$	$2b_1$ (Cl 3p)	8.75

[a] The VDE_1 value is shifted to align with the SO result in Table 2; [b] The energies of the X $^2B_2$ and a $^4B_1$ state are obtained from CCSD(T) calculations. The energies of higher doublet states relative to X $^2B_2$ and that of higher quartet states relative to the a $^4B_1$ state are obtained from CR-EOM-CCSD(T) calculations, respectively. The first two VDEs from SO CR-EOM-CCSD(T) are 5.18 and 5.25 eV, respectively.

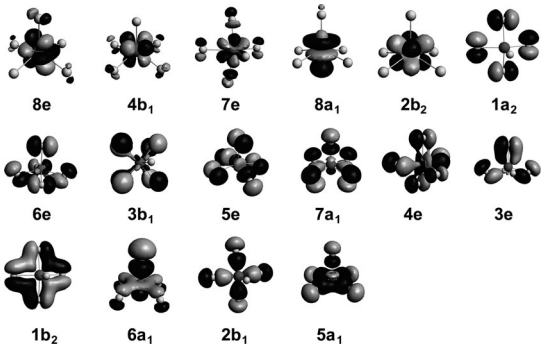

Figure 4. The contour diagrams of the frontier valence orbitals (α-spin orbitals) of UCl_5^- at the DFT/PBE level. The $8a_1$ and $2b_2$ orbital are singly occupied.

effects with a splitting of 0.4 eV (Figure 3) due to a small differential contribution from the U 6p orbitals, as found in other uranium halide compounds.[29–32] Qualitatively, the MO levels of UCl_5^- are similar to those of UF_5^-.[32] In addition, we also list some of the VDEs calculated with CR-EOM-CCSD(T) at the SR level in Table 3; the other VDEs are not available due to multi-reference characters of the higher detachment states.

Interpretation of the Photoelectron Spectra of UCl_5^-

Electron detachment from the two SOMOs ($8a_1$ and $2b_2$) yields the low binding energy features (X and *a*) in the PES spectra of UCl_5^-. The DFT/PBE calculation indicates that the VDEs for these two MOs are very close in energy with the VDE from the $2b_2$ MO higher by 0.18 eV, and CR-EOM-CCSD(T) gives the same trend with a 0.14 eV difference for the first two VDEs (Table 3). Even with the inclusion of SO effects in the DFT calculations (Figure 3), the first two VDEs remain close in energy, in good agreement with the observed band X and the weak shoulder *a* (Figure 2). Electron detachment from $8a_1$ ($5f_{z^3}$), the higher SOMO, results in the X band. The ADE of 4.76 eV observed for UCl_5^- is much higher than that of UF_5^- (3.885 eV),[32] indicating that UCl_5^- is highly electronically stable in the gas phase. Detachment from the $2b_2$ ($5f_{xyz}$) yields the weak *a* shoulder (Figure 2). This detachment channel was observed to have very low cross-sections in the case of UF_5^- and was not clearly observed because of the overlap with the X band.[32] The weak intensity of the *a* shoulder is consistent with the previous observation for UF_5^-.

Prior theoretical studies showed that Kohn–Sham orbitals and their orbital energies can be useful in the *qualitative* interpretation of electron detachments and spectroscopy properties.[33,34] Our previous experimental and theoretical results indicate that Koopmans' theorem holds approximately in molecules like uranyl halides[29,30] with aspects to the trend and the ordering of VDEs, although an overall energy shift is needed to compare with the experiment. In heavy metal complexes, state-specific methods with inclusion of SO effects are needed to accurately account for state energies. In the current work, we used both DFT and CR-EOM-CCSD(T) methods to interpret the PES spectra of UCl_5^-. The calculated VDEs at the SO-DFT/PBE level given in Table 3 are fitted with Gaussian functions to yield a simulated PES spectrum, which is compared with the 157 nm spectrum in Figure 5. The simulated spectral pattern

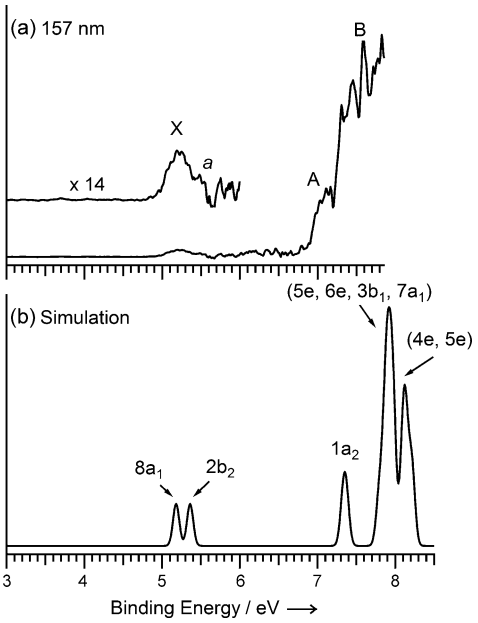

Figure 5. Photoelectron spectrum of UCl_5^- at 157 nm (a) in comparison with the simulated photoelecron spectrum at the SO-DFT/PBE level of theory (b). The simulated spectrum was generated by fitting a Gaussian of 0.04 eV width to each calculated VDEs, and the intensity of each detachment channel was set to be equal to one.

is in excellent agreement with the experimental data. Detachment from the nonbonding Cl 3p-based $1a_2$ MO in UCl_5^- (Figure 3 and 4) gives rise to band A with a very high VDE. Subsequently, detachment from the 5e, 6e, $3b_1$, $7a_1$, and 4e orbitals result in a series of closely spaced detachment channels, in agreement with the nearly continuous PES signals beyond 7.2 eV, labeled as B (Figure 2). The CR-EOM-CCSD(T) results of the first two VDEs with inclusion of the SO effects are 5.18 and 5.25 eV, respectively, in good agreement with the experiment. Given the negligible SO effects on the Cl 3p orbitals, the SR CR-EOM-CCSD(T) results for the higher VDEs derived from the Cl 3p lone-pair electron detachment are expected to undergo little SO splitting, except the 5e orbital. Compared to the SO-DFT/PBE results from the one-electron orbital picture, the SR CR-EOM-CCSD(T) method gives more detachment states in the energy range from 6.67 to 7.43 eV, which are in much better agreement with experimental bands A and B.

Structural Changes from UCl_5^- to UCl_5

The current study presents the first spectroscopic information on gaseous UCl_5 and UCl_5^- that can be used to verify the computational results. The calculated ground state of UCl_5 is a doublet state ($^2B_2$) with C_{4v} symmetry. The ADE of 4.73 eV at the CCSD(T)/SO level is in excellent agreement with the experimental value of 4.76 eV (Table 2). In addition, the ν_s(U−Cl_{ax}) stretching frequency of 353 cm^{-1} at the DFT level (Table 2) for the C_{4v} UCl_5 is also consistent with the observed approximately 350 cm^{-1} vibrational progression (Figure 2a). The 350 cm^{-1} ν_s(U−Cl_{ax}) vibrational frequency was exactly the value used to derive the bond dissociation energy $D°$ (Cl_4U−Cl) by Lau and Hildenbrand.[13] There have been significant previous efforts to estimate the vibrational frequencies of UCl_5, as well as the product of its three principal moments of inertia.[13,18–20,26] However, the results were not always consistent due to the assumptions about the geometry of UCl_5.[26] Therefore, the current findings lend considerable credence to the optimized structure and C_{4v} symmetry of UCl_5.

The optimized structural parameters for UCl_5 in the current work (Table 2) are consistent with the previous DFT/B3LYP result by Hay and co-workers.[26] The U−Cl_{ax} bond length of UCl_5 is 2.46 Å, which is slightly shorter than the U−Cl_{eq} bond length (2.48 Å). Upon removal of an electron from UCl_5^-, both DFT and CCSD(T) calculations show that the U−Cl bond lengths and $\sphericalangle Cl_{ax}UCl_{eq}$ angles of UCl_5 are reduced by about 0.1 Å and 3–6°, respectively. As seen in Figure 4, the $8a_1$ SOMO has very little contribution from the Cl 3p. Therefore, the shorter U−Cl bond lengths in neutral UCl_5 relative to those in UCl_5^- is mainly an electrostatic effect, due to the reduced intramolecular Coulomb repulsion in the neutral complex. The large bond length change is consistent with the observed vibrational progression in the PES spectrum (Figure 2a). The broad vibrational line width may suggest unresolved low frequency bending modes due to the bond angle change upon electron detachment.

Comparison with UF_5^-

The electron configuration of UCl_5^- is similar to that of UF_5^-,[26,27,32] with the two unpaired electrons occupying the U $5f_{z^3}$ and $5f_{xyz}$ orbitals in both systems. However, there are some subtle differences in the U-ligand bonding in the two systems. For UCl_5^-, the $8a_1$ SOMO ($5f_{z^3}$) has negligible contributions from the Cl 3p; there is only a minor 3p contribution at the axial Cl position (Figure 4). This small contribution in the SOMO might be related to the U−Cl_{ax} bond being longer by 0.03 Å in comparison to the U−Cl_{eq} bond (Table 2). In UF_5^-, however, the $8a_1$ SOMO ($5f_{z^3}$) has a small contribution from F 2p by all five ligands.[32] Consequently, both U−F_{ax} and U−F_{eq} bond lengths are almost equal, being about 2.136 and 2.138 Å, respectively. The exact percentage of the *n*p orbitals in the chemical bonding in UF_5^- and UCl_5^- will be discussed in detail in the next section. Overall, the U−Cl bond lengths (~2.56–2.59 Å) are much longer than the U−F bond lengths (~2.14 Å),[32] implying a weaker intramolecular Coulomb repulsion in the chloride complex and a higher ADE for UCl_5^- (4.76 eV) in comparison to that of UF_5^- (3.885 eV).[32] The smaller ADE of UF_5^- is due to its smaller size and the larger Coulomb repulsion by the fluoride ligands. We have observed that the detachment cross sections from the U $5f_{z^3}$ and $5f_{xyz}$ MOs are very small, in particular for the $5f_{xyz}$ MO. The current work shows that the detachment cross-sections from the 5f-based MOs are even lower in UCl_5^-, primarily due to the insignificant contributions from Cl 3p to these orbitals (Figure 4).

On the Trend of U−X Bonding in UX_5^- (X = F, Cl, Br, I): Ionic vs. Covalent Bonding

The experimental observation of gaseous UF_5^- and UCl_5^- provides an opportunity to investigate the periodic trend of the U−X bond for all the uranium pentahalide complexes UX_5^- (X = F, Cl, Br, I). Table 4 compares the U−X bond lengths, the natural charges, natural localized molecular orbitals (NLMOs), natural hybrid orbitals,[35] the Mayer,[36] Gopinathan–Jug (G–J),[37] and three types of Nalewajski–Mrozek (N–M) bond orders,[38] as well as the covalent contributions from natural resonance theory (NRT). The calculated NLMOs reveal that the U−X bonding has weak σ bonding interactions between the U dfσ and X spσ hybrid orbitals and weaker π bonding interactions between the U dfπ and X pπ orbitals. Both σ and π bonding interactions show an increasing contribution of the U 6d in the U−X bonding from F to I. The bond orders of U−X depend on the methods used, but generally increases from F to I. Only the N–M(2) method shows that the bond order of U−X is decreasing from F to I.

The natural population analysis (NPA) reveals that the covalent interaction in U−X becomes more important for heavier halogen ligands. Population analyses of the U atom show that the ionic character of U−X decreases from F to I; the charge on the U center changes from +2.27 in UF_5^- to +0.32 in UI_5^-. This trend can be seen from the significant

Table 4. Theoretical analyses of the U−X_{ax} bonds in UX_5^- (X = F, Cl, Br and I).[a]

	U−X_{ax}/Å	Q(U)	Q(X)	NLMO (β-spin)	Mayer	G–J	N–M(1)	N–M(2)	N–M(3)	Cov.(NRT)[b]
F	2.130	2.27	−0.67	4.4 % U($s^{0.36}d^{0.87}f$) + 95.5 % F($sp^{3.04}$) 2.9 % U($d^{0.30}f$) + 97.1 % F(p)	0.556	0.932	1.462	1.777	1.561	13.8 %
Cl	2.560	0.93	−0.39	8.6 % U($s^{1.14}d^{1.01}f$) + 91.3 % Cl($sp^{3.32}$) 4.1 % U($d^{0.33}f$) + 95.8 % Cl(p)	0.984	1.121	1.537	1.630	1.629	25.6 %
Br	2.724	0.64	−0.34	9.9 % U($s^{1.58}d^{1.29}f$) + 89.9 % Br($sp^{5.01}$) 4.1 % U($d^{0.41}f$) + 95.8 % Br(p)	0.853	1.142	1.542	1.612	1.634	29.4 %
I	2.939	0.32	−0.27	11.6 % U($s^{2.41}d^{1.69}f$) + 88.3 % I($sp^{6.33}$) 4.0 % U($d^{0.57}f$) + 95.9 % I(p)	1.114	1.214	1.571	1.584	1.660	30.6 %

[a] The N–M(1) and N–M(2) bond indices were calculated from two-electron valence indices based on partitioning of tr(ΔP^2) and were referred to as a 3-index and 4-index set, respectively. The N–M(3) bond order was calculated from valence indices based on partitioning of tr(PΔP). [b] Contribution of covalency to the NRT bond orders.

increase of the 6d and 7s population in the valence space of the U orbitals from X = F to I, while the population of the 5f orbital remains almost unchanged.[27] By contrast, the 5f orbitals have more contribution than 6d in UCl_6^{2-}, as shown in the literature.[39] For the total contribution of the X *n*p orbitals to the σ and π bonding interaction in UX_5^-, the F ligand leads the halogen group with 95.5 % and 97.1 %, respectively. The covalent interaction almost doubles from U−F (13.8 %) to U−Cl (25.6 %) and increases to 30.6 % for U−I. We note that the total percentage of 5f participation in the chemical bonding is only slightly increased as the bond covalency is enhanced. The covalency of the actinide-chlorine bonding has been previously discussed based on chlorine K-edge X-ray absorption spectroscopy (XAS) and ground-state and time-dependent hybrid density functional theory.[39]

Table 5 shows the calculated overlap integrals for the U 5f, 6d, 7s orbitals and the X *n*p group-orbitals for a_1 symmetry. Across the halogen series from F to I, the overlap integrals increase in magnitude between U 6d/7s and X *n*p, but decreases between U 5f and X *n*p. This trend is consistent with the enhanced U 6d, 7s characters in the σ-type and also π-type (in case of 6d) NLMOs of the U−X bonds. This result highlights the important role of U 6d and 7s participation in the U−X covalent bonding. The increase of the U−X bond covalency from F to I is mainly due to a better energy level matching between the U 6d, 7s and X sp orbitals and the subsequent larger orbital overlaps between the U 6d, 7s and the *n*p orbitals for the heavier halogen ligands. These findings are consistent with the previous calculations and the experimental results on the core and valence electrons of uranium halides.[16,26,27,39]

In order to understand the U−X binding strength and relevant energetics, we performed an energy decomposition analysis (EDA) for $UX_5^- \rightarrow UX_4 + X^-$ (X = F, Cl, Br, I) using DFT/PBE calculations, and the results are presented in Table 6. These calculations are performed on the optimized geometries of UX_5^- and the energies calculated are relevant to the UX_4 affinity of X^- ion. The affinity energies show that the UF_4–F^- bond is the strongest and the U−X bonds become weaker from X = F to I. The EDA results show that the U−F bond has the highest total steric interaction and the largest total orbital interaction. Thus, the additional strength of the U−F bond primarily comes from electrostatic interactions or ionic bonding. It is known from previous theoretical and thermodynamic studies that the U−F bond is the strongest among the uranium halides.[13,16,26,27,31,40] The current EDA result is consistent with the bond order trend by N–M(2), as presented in Table 4. The decreasing U−X bond strengths for heavier halogen ligands is due to the decreased steric interaction between U and X, as a result of the elongated U−X bonds. The decreased N–M(2) bond order and bond energies are consistent with the general trend of the bond dissociation energies from U−X.[41] The trend of the U−X bond strength in UX_5^- also follows the typical Badger-rule behavior,[42] that is, a longer bond results in a weaker bond energy. Therefore, the increasing U−X covalency from X = F to I does not guarantee a stronger bond because both ionic and covalent interactions are important. It should be pointed out that the various bond order calculations given in Table 4 do not predict the correct bonding trend, except for the N–M(2) method. All other bond order calculations show that the U−X bond order increases from F to I, which is contrary to the total bonding energies (Table 6).

Table 6. Energy decomposition analyses for $UX_5^- \rightarrow UX_4 + X^-$ (X = F, Cl, Br, I) from DFT/PBE calculations. All energies are in eV.

X	Steric Interaction			Orbital Interaction	Total Bonding Energy
	Electrostatic	Pauli	Sum[a]		
F	−7.41	5.63	−1.78	−4.35	−6.13
Cl	−5.68	4.79	−0.89	−4.03	−4.93
Br	−5.20	4.49	−0.72	−3.86	−4.58
I	−4.53	4.13	−0.40	−3.78	−4.18

[a] Steric interaction is the sum of the electrostatic and Pauli interactions.

Table 5. Calculated overlap integrals between the U 5f, 6d, 7s orbitals and the X *n*p group-orbitals with a_1 symmetry.

	X_{ax}-*n*p_z			X_{eq}-*n*$p_{x,y}$			X_{eq}-*n*p_z		
	U 5f	U 6d	U 7s	U 5f	U 6d	U 7s	U 5f	U 6d	U 7s
F	−0.0648	−0.1217	−0.0861	−0.0536	0.0718	−0.1677	−0.0653	−0.1632	0.0366
Cl	−0.0611	−0.1749	−0.1830	−0.0509	0.1070	−0.3572	−0.0564	−0.2021	0.0817
Br	−0.0574	−0.1860	−0.2124	−0.0471	0.1187	−0.4137	−0.0532	−0.2003	0.0928
I	−0.0522	−0.1963	−0.2466	−0.0419	0.1321	−0.4782	−0.0490	−0.1939	0.1039

Conclusions

In conclusion, we report a combined photoelectron spectroscopy and relativistic quantum chemistry study of UCl_5^- and UCl_5. The UCl_5^- complex is found to be highly electronically stable with an ADE of 4.76 eV, which is the electron affinity of neutral UCl_5. The ground state of UCl_5^- is a triplet with a $5f^2$ configuration, in which the two unpaired electrons occupy the primarily U $5f_{z^3}$ and $5f_{xyz}$ based MOs. The structures of UCl_5 and UCl_5^- are found both to be C_{4v}. The experimental results are interpreted on the basis of ab initio and DFT calculations. Extensive bonding analyses are performed for all uranium pentahalide complexes UX_5^- (X=F, Cl, Br, I) and reveal that ionic interactions are dominant in the U−F bond, while covalent interactions increase from X=F to I. The U−X bond strength decreases from F to I, as a result of the reduced electrostatic interactions, amid the increase of the relatively weak covalent interactions.

Experimental Section

Electrospray Ionization and Photoelectron Spectroscopy

The experiment was performed using an ESI-PES apparatus as described in detail previously.[43] The UCl_5^- anion was produced by electrospray ionization of a 1 mM solution of UCl_4 in acetonitrile. The anions from the ESI source were accumulated for 0.1 s in a cryogenically cooled ion trap operated at 20 K, and then pulsed into the extraction zone of a time-of-flight mass spectrometer. The UCl_5^- anions of interest were selected by a mass gate and decelerated before being intercepted by a laser beam in the detachment region of a magnetic-bottle photoelectron analyzer. In the current study, two photon energies were used: 157 nm (7.866 eV) from an F_2 excimer laser and 245 nm (5.061 eV) from a dye laser. The details of the cryogenically cooled ion trap has been described previously.[44] The cold ions are essential to eliminate vibrational hot bands and achieve better spectral resolution.[32b,43] The PES experiments were calibrated using the known spectra of Au^- and I^-. The Au^- atomic anion was produced by ESI of a acetonitrile solution of $[PPh_3AuCl]$ with $NaSCH_3$ and a trace amount of CH_3OH.[45] The electron kinetic energy resolution of the current magnetic-bottle photoelectron analyzer was about 3% (i.e., 30 meV for 1 eV electrons).[32,46]

Theoretical and Computational Methods

The theoretical studies were carried out using both density functional theory (DFT) and ab initio wavefunction theory (WFT) methods. DFT calculations were performed on UCl_5^- and UCl_5 using the generalized gradient approximation (GGA) with the PBE exchange-correlation functional[47] implemented in the Amsterdam Density Functional (ADF 2010.02) program.[48–50] The Slater basis sets with the quality of triple-ζ plus two polarization functions (TZ2P)[51] were used, with the frozen core approximation applied to the inner shells [$1s^2$-$5d^{10}$] for U and [$1s^2$-$2p^6$] for Cl. The scalar relativistic (SR) and spin-orbit (SO) coupling effects were taken into account by the zero-order-regular approximation (ZORA).[21] Geometries were fully optimized at the SR-ZORA level and single-point energy calculations were performed with inclusion of the SO effects via the SO-ZORA approach.

Advanced WFT electron correlation methods were used to obtain more reliable energies. The coupled-cluster with single and double and perturbative triple excitations [CCSD(T)] in MOLPRO 2008.1[52] and completely renormalized EOM-CCSD(T) (CR-EOM-CCSD(T))[53] in NWChem[54] were used in these calculations. The structures of UCl_5^- were optimized at the level of CCSD(T) with SR effects included, followed by a single-point CCSD(T) calculation of the ground state of UCl_5 at the optimized geometry of the anion, which accurately generated state-specific SR energies of the first vertical detachment energy (VDE). SO effects are significant for accurate ground-state energies due to the different number of unpaired 5f electrons before and after electron detachment. To obtain the SO correction on the ground-state energies, we performed CASSCF/CCSD(T)/SO calculations by including all the low-lying states arising from $5f^2$ of UCl_5^-, where the CCSD(T) excited state energies of UCl_5^- were obtained from CR-EOM-CCSD(T) excitation energies. This CASSCF/CCSD(T)/SO approach has been shown to produce accurate spin-orbit coupled excited state energies in previous studies.[28,31,55–59] We also used the CR-EOM-CCSD(T) method to obtain state-specific SR energies of some higher VDEs. In this approach, CR-EOM-CCSD(T) calculations were performed on the UCl_5 at the CCSD(T)-optimized geometry of the UCl_5^- to obtain the energies of the doublet and quartet excited states, with the CCSD(T) energy of the doublet and the quartet state corresponding to one electron removed from the $8a_1$ and $1a_2$ orbital, respectively, as reference. In the MOLPRO and NWChem calculations, we used the Stuttgart energy-consistent relativistic 32-valence-electron pseudopotentials ECP60 MWB (U) and the corresponding ECP60MWB-SEG basis for U,[60–62] and augmented polarized valence double-ζ basis sets aug-cc-pVDZ for Cl.[63] Because no cross-sections were calculated, the PES spectra were simulated by assuming that all the states have identical intensity.

Calculations of the bond orders of UX_5^- (X=F, Cl, Br, I) were carried out using ADF 2010.02. The basis sets TZ2P were used for F, Cl, Br, and I with the frozen core approximation applied to the inner shells [$1s^2$] for F, [$1s^2$-$2p^6$] for Cl, [$1s^2$-$3d^{10}$] for Br, and [$1s^2$-$4d^{10}$] for I. The geometry optimizations of UX_5^- (X=F, Br, I) were done at the PBE level. In addition, we employed natural bond orbital method[64] in the NBO 5.G program[65] to calculate natural localized molecular orbitals (NLMO), natural population analysis, and covalency analysis via natural resonance theory (NRT) to understand the bonding and electronic structures of UX_5^- (X=F, Cl, Br, I). The electronic wavefunction used for bonding analysis is from single-point DFT/B3LYP[66,67] calculations using Gaussian 09[68] at the DFT/PBE optimized geometries in the ADF calculations. In the Gaussian 09 calculations, we used the same pseudopotentials for U and the same basis sets for U and Cl as in the Molpro calculations,[60–62] the aug-cc-pVDZ.basis set for F,[69] the relativistic 25-valence-electron pseudopotential ECP10MDF (Br) and the corresponding aug-cc-pVDZ-PP for Br,[70] and the relativistic 25-valence-electron pseudopotential ECP28MDF (I) and the corresponding aug-cc-pVDZ-PP for I.[71]

Acknowledgements

This work was supported by the U.S. Department of Energy, Office of Basics Energy Sciences, and Division of Chemical Sciences, Geosciences, and Biosciences under Grant No. DE-FG02–11ER16261. The theoretical work was supported by NSFC (20933003, 11079006, 91026003) to JL and NSFC (21201106) and the China Postdoctoral Science Foundation (2012M520297) to JS. The calculations were performed using the DeepComp 7000 computer at the Supercomputer Center of the Computer Network Information Center, Chinese Academy of Sciences. A portion of the calculations was performed using EMSL, a national scientific user facility sponsored by the US Department of Energy's Office of Biological and Environmental Research and located at the Pacific Northwest National Laboratory, USA.

[1] C. Le Brun, *J. Nucl. Mater.* **2007**, *360*, 1–5.
[2] Y. H. Cho, T. J. Kim, S. E. Bae, Y. J. Park, H. J. Ahn, K. Song, *Microchem. J.* **2010**, *96*, 344–347.
[3] T. Nagai, A. Uehara, T. Fujii, O. Shirai, N. Sato, H. Yamana, *J. Nucl. Sci. Technol.* **2005**, *42*, 1025–1031.
[4] T. Nagai, A. Uehara, T. Fujii, N. Sato, H. Yamana, *IOP Conf. Ser. Mater. Sci. Eng.* **2010**, *9*, 012050.
[5] T. Nagai, A. Uehara, T. Fujii, O. Shirai, N. Sato, H. Yamana, *Electrochemistry* **2009**, *77*, 614–616.

[6] I. B. Polovov, V. A. Volkovich, J. M. Charnock, B. Kralj, R. G. Lewin, H. Kinoshita, I. May, C. A. Sharrad, *Inorg. Chem.* **2008**, *47*, 7474–7482.
[7] Y. H. Cho, S. E. Bae, Y. J. Park, S. Y. Oh, J. Y. Kim, K. Song, *Microchem. J.* **2012**, *102*, 18–22.
[8] L. Heerman, R. De Waele, W. D'Olieslager, *J. Electroanal. Chem.* **1985**, *193*, 289–294.
[9] G. Prins, E. H. P. Cordfunke, *Thermochim. Acta* **1982**, *57*, 109–111.
[10] H. Martin, K. H. Eldau, *Z. Anorg. Allg. Chem.* **1943**, *251*, 295–304.
[11] J. J. Katz, E. Rabinowitch in *The Chemistry of Uranium*, NNES, VIII-5, McGraw-Hill Book Co. Inc., New York, NY, **1951**, pp. 496, 497.
[12] D. M. Gruen, R. L. McBeth, *Inorg. Chem.* **1969**, *8*, 2625–2633.
[13] K. H. Lau, D. L. Hildenbrand, *J. Chem. Phys.* **1984**, *80*, 1312–1317.
[14] G. S. Smith, Q. Johnson, R. E. Elson, *Acta Crystallogr.* **1967**, *22*, 300–303.
[15] K. Fuji, C. Miyake, S. Imoto, *J. Nucl. Sci. Technol.* **1979**, *16*, 207–2013.
[16] E. Thibaut, J.-P. Boutique, J. J. Verbist, J.-C. Levet, H. Noël, *J. Am. Chem. Soc.* **1982**, *104*, 5266–5273.
[17] C. Miyake, K. Fuji, S. Imoto, *Inorg. Nucl. Chem. Lett.* **1977**, *13*, 53–55.
[18] R. C. Paul, G. Singh, M. Singh, *J. Inorg. Nucl. Chem.* **1971**, *33*, 713–720.
[19] J. Selbin, J. D. Ortego, G. Gritzner, *Inorg. Chem.* **1968**, *7*, 976–982.
[20] K. W. Bagnall, D. Brown, J. G. H. du Preez, *J. Chem. Soc.* **1965**, *0*, 5217–5221.
[21] E. van Lenthe, E. J. Baerends, J. G. Snijders, *J. Chem. Phys.* **1993**, *99*, 4597–4610.
[22] W. Küchle, M. Dolg, H. Stoll, H. Preuss, *J. Chem. Phys.* **1994**, *100*, 7535–7542.
[23] P. J. Hay, R. L. Martin, *J. Chem. Phys.* **1998**, *109*, 3875–3881.
[24] G. Schreckenbach, *Inorg. Chem.* **2000**, *39*, 1265–1274.
[25] G. Schreckenbach, G. A. Shamov, *Acc. Chem. Res.* **2010**, *43*, 19–29.
[26] E. R. Batista, R. L. Martin, P. J. Hay, *J. Chem. Phys.* **2004**, *121*, 11104–11111.
[27] J. E. Peralta, E. R. Batista, G. E. Scuseria, R. L. Martin, *J. Chem. Theory Comput.* **2005**, *1*, 612–616.
[28] a) L. S. Wang, X. B. Wang, *J. Phys. Chem. A* **2000**, *104*, 1978–1990; b) X. B. Wang, X. Yang, L. S. Wang, *Int. Rev. Phys. Chem.* **2002**, *21*, 473–498; c) X. B. Wang, L. S. Wang, *Annu. Rev. Phys. Chem.* **2009**, *60*, 105–126.
[29] P. D. Dau, J. Su, H. T. Liu, J. B. Liu, D. L. Huang, J. Li, L. S. Wang, *Chem. Sci.* **2012**, *3*, 1137–1146.
[30] P. D. Dau, J. Su, H. T. Liu, D. L. Huang, J. Li, L. S. Wang, *J. Chem. Phys.* **2012**, *137*, 064315.
[31] J. Su, P. D. Dau, Y. H. Qiu, H. T. Liu, C. F. Chao, D. L. Huang, L. S. Wang, J. Li, *Inorg. Chem.* **2013**, *52*, 6617–6626.
[32] a) P. D. Dau, J. Su, H. T. Liu, D. L. Huang, F. Wei, J. Li, L. S. Wang, *J. Chem. Phys.* **2012**, *136*, 194304; b) P. D. Dau, H. T. Liu, D. L. Huang, L. S. Wang, *J. Chem. Phys.* **2012**, *137*, 116101.
[33] a) R. Stowasser, R. Hoffmann, *J. Am. Chem. Soc.* **1999**, *121*, 3414–3420; b) P. Politzer, F. Abu-Awwad, *Theor. Chem. Acc.* **1998**, *99*, 83–87.
[34] D. P. Chong, O. V. Gritsenko, E. J. Baerends, *J. Chem. Phys.* **2002**, *116*, 1760–1772.
[35] A. E. Reed, L. A. Curtiss, F. Weinhold, *Chem. Rev.* **1988**, *88*, 899–926.
[36] I. Mayer, *Chem. Phys. Lett.* **1983**, *97*, 270–274.
[37] M. S. Gopinathan, K. Jug, *Theor. Chim. Acta* **1983**, *63*, 497–509.
[38] a) A. Michalak, R. L. DeKock, T. Ziegler, *J. Phys. Chem. A* **2008**, *112*, 7256–7263; b) R. F. Nalewajski, J. Mrozek, *Int. J. Quantum Chem.* **1994**, *51*, 187–200; c) R. F. Nalewajski, J. Mrozek, *Int. J. Quantum Chem.* **1997**, *61*, 589–601; d) R. F. Nalewajski, J. Mrozek, A. Michalak, *Polish J. Chem.* **1998**, *72*, 1779–1791; e) R. F. Nalewajski, J. Mrozek, G. Mazur, *Can. J. Chem.* **1996**, *74*, 1121–1130.
[39] S. G. Minasian, J. M. Keith, E. R. Batista, K. S. Boland, C. N. Christensen, D. L. Clark, S. D. Conradson, S. A. Kozimor, R. L. Martin, D. E. Schwarz, D. K. Shuh, G. L. Wagner, M. P. Wilkerson, L. E. Wolfsberg, P. Yang, *J. Am. Chem. Soc.* **2012**, *134*, 5586–5597.
[40] M. Straka, M. Patzschke, P. Pyykkö, *Theor. Chem. Acc.* **2003**, *109*, 332–340.
[41] J. W. Bruno, H. A. Stecher, L. R. Morss, D. C. Sonnenberger, T. J. Marks, *J. Am. Chem. Soc.* **1986**, *108*, 7275–7280.
[42] a) R. M. Badger, *J. Chem. Phys.* **1934**, *2*, 128–132; b) R. M. Badger, *Phys. Rev.* **1935**, *48*, 284–285; c) R. M. Badger, *J. Chem. Phys.* **1935**, *3*, 710–715.
[43] L. S. Wang, C. F. Ding, X. B. Wang, S. E. Barlow, *Rev. Sci. Instrum.* **1999**, *70*, 1957–1966.
[44] X. B. Wang, L. S. Wang, *Rev. Sci. Instrum.* **2008**, *79*, 073108.
[45] C. G. Ning, X. G. Xiong, Y. L. Wang, J. Li, L. S. Wang, *Phys. Chem. Chem. Phys.* **2012**, *14*, 9323–9329.
[46] H. T. Liu, Y. L. Wang, X. G. Xiong, P. D. Dau, Z. Piazza, D. L. Huang, C. Q. Xu, J. Li, L. S. Wang, *Chem. Sci.* **2012**, *3*, 3286–3295.
[47] J. P. Perdew, K. Burke, M. Ernzerhof, *Phys. Rev. Lett.* **1996**, *77*, 3865–3868.
[48] ADF 2010.01, http://www.scm.com.
[49] C. Fonseca Guerra, J. G. Snijders, G. te Velde, E. J. Baerends, *Theor. Chem. Acc.* **1998**, *99*, 391–403.
[50] G. te Velde, F. M. Bickelhaupt, E. J. Baerends, C. F. Guerra, S. J. A. van Gisbergen, J. G. Snijders, T. Ziegler, *J. Comput. Chem.* **2001**, *22*, 931–967.
[51] E. van Lenthe, E. J. Baerends, *J. Comput. Chem.* **2003**, *24*, 1142–1156.
[52] H. J. Werner, P. J. Knowles, R. Lindh, F. R. Manby, M. Schütz, others. MOLPRO, version 2008.1, a package of ab initio programs, see http://www.molpro.net.
[53] K. Kowalski, P. Piecuch, *J. Chem. Phys.* **2004**, *120*, 1715–1738.
[54] M. Valiev, E. J. Bylaska, N. Govind, K. Kowalski, T. P. Straatsma, H. J. J. Van Dam, D. Wang, J. Nieplocha, E. Apra, T. L. Windus, W. de Jong, *Comput. Phys. Commun.* **2010**, *181*, 1477–1489.
[55] X. B. Wang, Y. L. Wang, J. Yang, X. P. Xing, J. Li, L. S. Wang, *J. Am. Chem. Soc.* **2009**, *131*, 16368–16370.
[56] Y. L. Wang, H. J. Zhai, L. Xu, J. Li, L. S. Wang, *J. Phys. Chem. A* **2010**, *114*, 1247–1254.
[57] Y. L. Wang, X. B. Wang, Y. X. P. Xing, F. Wei, J. Li, L. S. Wang, *J. Phys. Chem. A* **2010**, *114*, 11244–11251.
[58] H. T. Liu, X. G. Xiong, P. D. Dau, Y. L. Wang, J. Li, L. S. Wang, *Chem. Sci.* **2011**, *2*, 2101–2108.
[59] J. Su, Y. L. Wang, F. Wei, W. H. E. Schwarz, J. Li, *J. Chem. Theory Comput.* **2011**, *7*, 3293–3303.
[60] http://www.theochem.uni-stuttgart.de/pseudopotential.
[61] X. Cao, M. Dolg, H. Stoll, *J. Chem. Phys.* **2003**, *118*, 487–496.
[62] X. Cao, M. Dolg, *THEOCHEM* **2004**, *673*, 203–209.
[63] D. E. Woon, T. H. Dunning, *J. Chem. Phys.* **1993**, *98*, 1358–1371.
[64] F. Weinhold, C. R. Landis in *Valency and Bonding. A Natural Bond Orbital Donor-Acceptor Perspective*; Cambridge University Press, Cambridge, UK, **2005**.
[65] E. D.Glendening, J. K. Badenhoop, A. E. Reed, J. E. Carpenter, J. A. Bohmann, C. M. Morales, F. Weinhold, *NBO 5.G*; Theoretical Chemistry Institute, University of Wisconsin: Madison, WI, **2004**; http://www.chem.wisc.edu/~nbo5.
[66] A. D. Becke, *Phys. Rev. A* **1988**, *38*, 3098–3100.
[67] C. Lee, W. Yang, R. G. Parr, *Phys. Rev. B* **1988**, *37*, 785–789.
[68] Gaussian 09, revision B.01, M. J. Frisch, et al. Gaussian, Inc.: Wallingford, CT, **2010**.
[69] R. A. Kendall, T. H. Dunning, R. J. Harrison, *J. Chem. Phys.* **1992**, *96*, 6796–6806.
[70] K. A. Peterson, D. Figgen, E. Goll, H. Stoll, M. Dolg, *J. Chem. Phys.* **2003**, *119*, 11113–11123.
[71] K. A. Peterson, B. C. Shepler, D. Figgen, H. Stoll, *J. Phys. Chem. A* **2006**, *110*, 13877–13883.

Received: May 3, 2013
Published online: July 12, 2013